AXIAL-MOMENT INTERACTION FOR 2D WELDED STEEL JOINTS USING FEA: AN INITIAL INVESTIGATION

Eduardo Bayo,
University of Navarra. Spain

Javier Gracia
University of Oviedo. Spain.

Jeppe Jönsson
DTU Technical University of Denmark.

ABSTRACT

A systematic finite element based approach is presented to characterize the interaction between the bending moments and axial forces coming from the connected beams in 2D welded steel joints. The modeling technique is described in the paper, as well as the description of the interaction diagrams between axial forces and bending moments for a series of commercial steel sections. An initial imperfection is included in the finite element model to capture the possible buckling failure modes in the column web and the beam flanges. The approach predicts moment capacities that are very similar to those predicted by Eurocode 3 in the absence of axial forces. Interaction diagrams and moment rotation curves are shown for different levels of axial forces, as well as axial force versus displacements for different levels of bending moments. An investigation is also carried out that shows that the approach leads to axial-bending interaction curves that are path independent. Finally, a nonlinear exponential curve fitting is proposed for the axial-moment interaction diagram.

Keywords: welded steel joints; axial-bending interaction diagrams; path independent plastic behaviour; nonlinear exponential curve fitting; limit surfaces;

1. INTRODUCTION

The most common way to characterize the behaviour of steel connections is by means of moment-rotation curves. They provide information on the initial stiffness, moment resistance and rotation capacity. The component method has been proposed in Eurocode 3 (EC3) Part 1.8 [1] to provide such information, which is subsequently used in frame analyses by means of rotational springs. Reference [2] provides a good background document and design manual for connections according to EC3. There are a number of situations in which the axial forces may become significant in beam to column connections. Such situations include: sway frames subject to large lateral forces produced by strong wind conditions and/or earthquakes; Vierendeel type of beams that avoid diagonal elements; beam splices; irregular frames under gravity and lateral forces; and structures under fire conditions or subject to progressive collapse.

Part 1.8 of EC3 proposes the calculation of the moment resistance neglecting the axial interaction provided that the acting axial load does not exceed 5% of the axial design resistance of the connected beam, otherwise a linear axial-bending interaction relation is supposed to be used. This linear relation involves the axial resistance of the connection assuming there is no moment, however neither formula nor indications are given in EC3 Part 1.8 as how to calculate such resistance in either tension or compression.

Previous studies have addressed the interaction between the axial force and bending moment in steel joints [3-10]. Most of this work deals with two main issues: experimental studies to characterize the possible interactions; and component based analytical and mechanical models. The results of an experimental program that included extended plate beam-to-column connections were presented in [3]. The researchers concluded that the presence of the axial force should be considered in the joint design. In [4] experimental results were also presented for flushed end-plate beam-to-column connections. A common conclusion of the results of these works was that the presence of axial forces has an important effect on the joint bending response,

and along with it the need to define an interaction between them. Component based mechanical models, that include axial and moment interaction of 2D connections, have been proposed in [4-10]. The reader is referred to [8] for a comprehensive description of different models and experimental work. Recently a comprehensive method, based on an assembly procedure of components, has been proposed by Demonceau et al [9] to characterize N-M interactions. In addition, it was found that the 5% rule leads to an overestimation of the moment capacity in the 5% band, while the linear part of the rule is rather conservative. Similar findings are also observed in this study, as it will be shown below. Another component-based method has been recently proposed by Gil-Martin et al. [10], which also includes axial-bending interaction. Also in the context of connections for spatial lattice structures experimental and analytical models have been presented in [11-13]. Again, the conclusions point out to the importance of the axial-moment interaction in the resistance of the joint and the need to consider it in the global structural analysis.

Three dimensional finite element models have been widely used in steel joint analysis [14-20] for the characterization of their properties, and the assessment of local effects. They have also been used to perform numerous parametric analyses to validate analytical procedures. The finite element method (FEM) has worked very well in the simulation of bolted [14-16] as well as welded connections [17-20] using different types of elements (shell and solid) and computer programs, and it is widely considered as a very accurate and reliable technique to characterize the complete behaviour of steel joints.

In this paper an efficient method is proposed to obtain accurate axial-moment interaction curves of 2D steel connections. The method is based on detailed and accurate finite element models, and offers an alternative to the component method for those who prefer to characterize connections using finite element models. The modelling procedure proposed in [21] for stiffness characterization, is expanded and enhanced herein to make it suitable for resistance evaluations

in which both, bending moments and axial forces concur at the steel connection. In this way, axial force versus bending moment interaction diagrams can be obtained readily. The effects of the shear force in the web panel and column longitudinal axial force have not been considered in this study. Section 2 explains the finite element modelling process and the rigid surface constraint procedure to introduce the bending moment and axial forces. The consideration of initial imperfections and model validation are also described in Section 2. Section 3 includes the generation of N-M interaction diagrams for tension and compression, and a study that shows that the limit surfaces are path independent, and can be well approximated using a nonlinear exponential curve fitting technique. Finally, some conclusions are drawn in Section 4.

2. FINITE ELEMENT MODEL

In this section a systematic finite element modelling procedure is presented to characterize the resistance of the steel connection in terms of the axial-bending interaction. The ABAQUS program has been used to construct the finite element models of the steel joints. Then a rigid surface constraint procedure has been implemented to introduce the axial and bending moments in the simulation process.

2.1 Finite element model and surface constraints

In this research, welded steel joints have been modelled using similar finite element procedures to those already used by different authors and researchers, which were corroborated against experimental tests giving very good results (see references [18-20]). The joints have been modelled with 8 node C3D8R solid finite elements that include reduced integration (to avoid shear locking) and hourglass control (see Fig. 1). The full penetration butt welds between columns and beams have been considered using a kinematic type of constraint condition allowed by ABAQUS. The beam section has been declared as the “master surface” while the column flange as the “slave”.

As shown in Fig. 1, for a HEB 200 column and an IPE 330 beam, the FE model has been prolonged at each side of the columns and beams. The reason for these elongations is to guarantee that the limits of the model are long enough to capture the areas of stress concentrations that appear in the lower and upper part of the beam web panel next to the column flange, as well as the column web panel. In addition, the possible failure modes of the beam flange in compression and tension are also taken into consideration in this way. A parametric study carried out in [21] confirmed that *h/5* (where *h* is the depth of the connected beam) is long enough to capture these effects. The complete finite element model depicted in Fig. 1, has a minimum element size of 2.5 millimetres, a maximum size of 5 millimetres, and a total of 217,680 degrees of freedom (DOF). It was shown in [21] that this type of finite element model provides very good results for stiffness characterization. In what follows, it will be explained how the model has been expanded and enhanced to include non-linear properties as well as initial imperfections to characterize the resistances and obtain axial-bending interaction diagrams.

The beam deformation hypotheses have been introduced at the boundary of the joint model to ensure that these sections remain plane after deformation. In order to impose these hypotheses, sections A, B, C and D in the finite element model (see Fig. 1) have been constrained to displace as rigid surfaces. Thus, the horizontal and vertical displacements, as well as the rotation of the nodes in these surfaces have been tied to those of their reference points (centres of gravity) of the respective sections A, B, C and D. This also allows introducing in a straightforward way the axial forces and bending moments at sections C and D. In order to constraint the rigid body motions section C has been pinned, and a roller has been situated in section D as shown in Fig. 2. In this way, section D carries the combination of bending moment and axial force whose interaction will be presented below in this paper. The shear interaction is avoided by introducing in section C a moment of equal value and opposite sign to that introduced in section D.

The material behaviour has been introduced in the finite element model by means of an elastic perfectly plastic stress-strain relation as indicated in EC3 Part1-5 [22], along with the Von Misses yield criteria. The types of steel used for this study are S275 and S355; and the values adopted for the elastic modulus E and the Poisson ratio ν have been 21000 kN/cm^2 and 0.3, respectively. Material and geometric non-linear analysis have been performed in all cases using Riks method as the solution control algorithm, which allows for the analysis of limit and post-limit state responses.

2.2 Consideration of initial imperfections

The bending moment and axial compressive force produce normal stresses in the column web and beam flange, which may lead to their buckling failure. In order to capture this effect an initial imperfection has been introduced, as specified in Eurocode 3 Part 1.5 [22], by scaling the first buckling mode due to axial loading acting in the beam by a factor of l/200, where l is the of the minimum of the column web panel width or beam depth. This scaling factor is considered fairly conservative as reported in [23]. Fig. 3a shows the enlarged shape of such initial imperfection for the case of a HEB 200 column and an IPE 330 beam. This initial imperfection has been chosen because the axial-moment diagrams have been generated by imposing first a reference beam axial load (in tension and/or compression), and then by increasing the bending moment coming from the beam until failure.

Nevertheless, a study has been made to see the possible differences when using an initial buckling mode imperfection generated by beam bending loading. Such a buckling mode is shown in Fig. 3b (**JAVI POR FAVOR INTRODUCE ESTA FIGURA**). The following beam-to-column joints have been considered: HEB200-IPE330; HEB260-IPE400; and HEB300-IPE500, with the HEB for the columns and the IPE for the beams.

Figs. 4 shows the three sets of moment-rotation curves corresponding to the different beam-to-column joints mentioned above. For each joint, one case corresponds to the axial buckling mode scaled by a factor of $l/200$; another to the bending buckling mode also scaled by a factor of $l/200$; and the last one corresponds to the bending buckling mode scaled by $l/10^5$, which is a very small deformation. It may be observed that the three different bucking shapes lead to the same bending resistance for each of the different joints. Both the axial and bending buckling shapes scaled by $l/200$ give the same limit and post-limit behaviour; in fact the curves overlap each other. In the case of the buckling shape with a scale factor of $l/10^5$ the resistance is the same but the post-limit behaviour is different with practically no softening. The use of these imperfections will give results that are on the safe side for those cases in which the imperfections are restrained by beams connected to the column web.

Similar to the moment resistance, Fig. 5 depicts the tension force versus displacements for the three different sets of beam-column joints and initial imperfections. The tension resistance curves also show the same resistances and again the axial and bending buckling shapes yield the same results. Fig. 5 also demonstrates that in the case of a tension force the influence of the initial imperfection is insignificant.

Finally, Fig. 6 illustrates the compression force versus displacement curves. These curves now show the importance of the imperfection amplitude, since the behaviour with no imperfection is different from that of the imperfections with larger amplitude. However, the shape of the imperfection is not important, in fact, similar to the previous cases, the curves resulting from axial and bending imperfections overlap each other, and the only difference is that the axial buckling mode leads to a bit of less resistance than the bending buckling mode. The post-limit behaviour is the same in both cases. As a consequence, the axial buckling mode can be considered slightly more conservative than the bending one, and this is an additional reason why it has been adopted in this study.

2.3 Model verification and validation

The proposed finite element model has been verified by comparing the moment resistances of a series of beam-to-column joints obtained by this method and the predictions given by EC3 Part 1.8 [1]. It has also been validated by comparing this method with the experimental results reported in [17].

Eurocode 3 Part 1.8 predicts the moment resistance, with no axial force, of a welded connection based on the following criteria: column web in transverse compression (described in Clause 6.2.6.2); column web in transverse tension (Clause 6.2.6.3); column flange in transverse bending (Clause 6.2.6.4), and beam flange and web in compression (Clause 6.2.6.5).

The beam-to-column cases included in Table 1 have been analysed using the proposed method as explained above. The moment-rotation curves have been obtained and examined to get the moment resistance M_{Rd}. Such resistance has been found, as proposed in [13], by measuring the moment (M_p in the figure) at the point of intersection of the moment-rotation curve with the tangent of slope S_p equal to 20% of the initial stiffness $S_{j,ini}$ (see Fig. 7). Table 1 shows the results of the comparison and the component that fails; *cwc* and *bfc* mean column web in compression, and beam flange in compression, respectively. For the majority of the cases the failure mode is the web panel under compression. Both the proposed method and EC3 predict the same component failure. Relative errors in the moment resistance are also shown in Table 1: the average relative error is 1.8% and the maximum relative error is 4.7%. These low errors and prediction of the component failure lead the authors to conclude that the proposed numerical method gives similar predictions to those obtained by the Eurocode 3.

The experimental cases described in [17] have also been analysed using the proposed finite element approach. The experimental tests were performed applying compressive loads to the webs of commercial steel sections. Table 2 illustrates the characteristics and results obtained experimentally as reported in [17], and by the proposed numerical finite element method. The

maximum error is 6.3%, and this also leads to conclude that the finite element model replicates the results of the tests with sufficient precision.

3. AXIAL-MOMENT INTERACTION CURVES

Once the model has been validated, a series of cases of different beam-to-column joints have been analysed to obtain the interaction curves. Fig. 8 shows these curves obtained for the joints used in Section 2.2: HEB200-IPE330; HEB260-IPE400; and HEB300-IPE500 under axial tension force and bending moment. The left side of Fig. 8 shows the interaction curves M versus N_t (tension) and the right one shows the normalized curves M/M_{Rd} and $N_t/N_{t,Rd}$, where M_{Rd} is the maximum moment obtained when N_t is equal to zero, and $N_{t,Rd}$ is the maximum force obtained in the absence of bending moment M. These diagrams have been smoothed between the sampling points. The way in which the interaction curves have been obtained is by first finding $N_{t,Rd}$ by increasing the axial load, with no moment, until failure; and afterwards by imposing the following axial load levels as a percentage of $N_{t,Rd}$: 0, 10%, 25%, 50% and 75%. With these axial loads fixed, the bending moments have been increased until failure, and the case when N_t=0 renders M_{Rd}. It is important to notice how the normalized curves practically superimpose with each other. This fact is going to be considered at the time of developing a nonlinear exponential fitting in Section 3 below.

It is also important to notice at this stage the difference of the obtained interaction curves with that proposed in EC3 Part 1.8, which is included in the normalized interaction diagram of Fig. 8 as a diagonal line with the 5% limit region. It is apparent that the EC3 is rather conservative in the linear part of the curve; this result is in agreement with the findings in [10]. ~~for low axial forces, which are the most common cases.~~ For 10% of axial load level the EC3 predicts a 90% for the moment resistance (linear interaction), whereas the proposed approach yields 99%. Also for 20% of axial load the EC3 predicts 80% of the moment resistance and the proposed method results in 96%.

Fig. 9 presents the interaction diagrams for the axial compression case, and again the same trend is detected when it comes to the normalized curves. For 10% of axial load level the EC3 predicts a 90% for the moment resistance (linear interaction), whereas the proposed approach yields 98%; and for 20% of the axial load, the EC3 predicts 80% of the moment resistance and the proposed method results in a 94% prediction.

Figs. 10, 11 and 12 show the moment rotation curves for the different levels of axial load (0; 10%, 25%, 50% and 75%) for the HEB200-IPE330; HEB260-IPE400; and HEB300-IPE500 joints, respectively. The left side shows the tension case, and the right side shows the compression case. It may be observed how the moment resistance decreases when increasing the axial loads, and how the softening post limit behaviour becomes more accentuated with increasing compressive loads. It may also be observed how the initial rotational stiffness does not change with respect to the amount of axial load for both tension and compression.

Fig. 13 shows the force-displacement curves for the different levels of bending moments for the HEB200-IPE330 joint. The left and right sides show the tension case and the compression case, respectively. It may be observed how the axial resistance decreases when increasing the bending moments, and how the softening post limit behaviour for the case of compression becomes more accentuated with increasing moment loads. It may also be seen how the initial stiffness does not change with respect to the amount of bending load for both tension and compression. The behaviour for the joints HEB260-IPE400 y HEB300-IPE500 is very similar to that of the HEB200-IPE330 joint and it is not worth repeating.

3.1 Path dependency

In order to assess if the interaction diagrams are path dependant, the loading pattern is reversed to generate new interaction diagrams. Now, the moments are fixed and the axial forces are increased until failure. The maximum moments that were obtained for the axial levels of 10%, 25%, 50% and 75% are now fixed and the axial loads (in tension and compression) are

increased until reaching the limit surface. In other words, the limit diagrams have been obtained by following two different paths: a vertical loading path (increasing the moments) and a horizontal loading path (increasing the axial forces).

Tables 3 and 4 show the limit values of the interaction curves obtained by both methods for the HEB200-IPE330 joint under tension and compression, respectively. The results are given in absolute as well as in normalized values. It can be observed how these values are very similar thus showing no dependency on the loading pattern. Similarly Tables 5 and 6 show the values of the interaction curves obtained by both methods for the HEB260-IPE400 joint under tension and compression, respectively. Tables 7 and 8 show those values for the joint HEB300-IPE500. The results are again given in absolute as well as in normalized values, and it can be seen again how these values are practically the same, thus showing no dependency on the loading pattern. With these results it is concluded that the interaction curves obtained by the proposed method are for all practical purposes path independent.

3.2 Behaviour model

The normalized axial-moment interaction curves for the joints included in Table 1 are shown in Fig. 14 for tension (left) and compression (right). Fig. 14 also shows the 5% rule and the linear diagonal interaction proposed in EC3 Part 1.8. One can see that the pattern of the interaction curves is quite uniform, and that all of them practically superimpose each other within a narrow band. For each one of the curves a nonlinear exponential fitting as defined by Equation 1 has been developed using the function *fitnlm* of Matlab [21] to fit nonlinear models.

$$\left(\frac{N}{N_{Rd}}\right)^{\alpha}+\left(\frac{M}{M_{Rd}}\right)^{\beta}=1 \qquad (1)$$

The average values that have been obtained from the sample cases for the case of bending moment versus axial tension are: $\alpha = 2.05$ and $\beta = 0.86$. In the case of the interaction between bending moment and axial compression the average values are: $\alpha = 1.55$ and $\beta = 1.20$. These two

cases are represented in Fig. 14 by a solid line. This type of nonlinear fit is adequate for this family of 2D welded connections. Other types of connections may require a different fit, and this will be studied in future works.

4. CONCLUDING REMARKS

The aim of this study has been to propose a systematic and accurate finite element based approach to characterize the interaction between the bending moments and axial forces coming from the connected beams in 2D welded steel joints. The approach predicts moment capacities that are very similar to those predicted by Eurocode 3 in the absence of axial forces. In addition, the main conclusions from this research can be summarized as follows:

1. The proposed finite element modelling technique is based on a finite element mesh with constrained surface conditions, and an initial imperfection to correctly capture the possible buckling failure modes in the column web as well as the beam flanges.
2. The proposed modelling process leads to axial-bending interaction curves that are path-independent. The same results are obtained by fixing the axial force and incrementing the moments (vertical path), and by fixing the moment and increasing the axial force (horizontal path).
3. A nonlinear exponential curve characterises the axial-moment interaction with good precision for the family of cases contemplated in this research.
4. It has been observed from the moment rotation curves, that the level of axial loading coming from the connected beam has a strong influence on the moment resistance and post-limit behaviour. The compressive axial forces reduce significantly the rotation capacity and increase the softening post-limit effect. However, the initial rotational stiffness does not seem to be affected by the level of axial loading.
5. For the welded connections that have been studied in this research, the *N*-*M* interaction proposed by Eurocode 3 becomes rather conservative in the linear part, however it tends to

overestimate the resistance in the 5% bracket. However, this research corroborates the Eurocode 3 assertion that the connection has limited ductility when subject to moment and axial compressive forces.

6. This study has been an initial investigation on axial-moment interaction on steel connections. The combination of axial-moment in the connection with the shear and axial forces acting in the column web panel warrant a separate study that will become part of future research.
7. The scope of the proposed method can be enlarged and applied to other kind of joints and loading conditions, and predictive models can be explored based on machine learning techniques [25-26]. These will also be part of future investigations.
8. The proposed results could be easily implemented in structural analysis programs, and facilitate the analysis and design of welded steel frames and joints. In fact, the proposed approach complements and enhances the stiffness model proposed in [21] by adding the joint resistance and interaction diagrams to the cruciform element developed therein. In the context of advanced structural analysis proposed in modern codes, the proposed method could be useful since it allows the joint to be precisely modelled within the structural system.

ACKNOWLEDGEMENTS

The financial support provided to the first author through the program Salvador de Madariaga of the Ministerio de Ciencia, Innovación y Universidades with reference number PRX18/00094 for a research stay at DTU; as well as the support from the Spanish Ministerio de Economía, Industria y Competitividad-Agencia Estatal de Investigación y Fondo Europeo de Desarrollo Regional under contract BIA2016-80358-C2-1-P MINECO/FEDER UE are gratefully acknowledged.

REFERENCES

[1] CEN. Eurocode 3: Design of Steel Structures. Part 1.8: Design of Joints (EN 1993-1-8), 2005.

[2] Jaspart J.P, Weynand K. *Design of joints in steel and composite structures*. ECCS – European Convention for Constructional Steelwork 2016.

[3] Lima LRO, de Simoes da Silva L, Vellasco PCGS, de Andrade SA. Experimental evaluation of extended end-plate beam-to-column joints subjected to bending and axial force. Engineering Structures 2004; 26:1333–1347.

[4] Simões da Silva L, de Lima LRO, Vellasco PCGS, de Andrade SA. Behaviour of flush end-plate beam-to-column joints under bending and axial force. Steel and Composite Structures 2004; 4(2): 77–94.

[5] Simões da Silva L, Coelho AMG. An analytical evaluation of the response of steel joints under bending and axial force. Computers & Structures 2001; 79: 873–881.

[6] Sokol Z, Wald F, Delabre V, Muzeau J-P, Svarc M. Design of endplate joints subject to moment and normal force. In: Third European conference on steel structures. Eurosteel 2002. Coimbra: Cmm Press; 2002. p. 1219–1228.

[7] Urbonas K, Daniunas A. Behaviour of semi-rigid steel beam-to-beam joints under bending and axial forces. Journal of Constructional Steel Research 2006; 62:1244–1249.

[8] Del Savio A.A., Nethercot D.A., Vellasco P.C.G.S, Andrade S.A., Martha L. Generalised component-based model for beam-to-column connections including axial versus moment interaction, Journal of Constructional Steel Research 2009; 65: 1876–1895

[9] Demonceau J.F, Cerfontaine F, Jaspar J.P. Resistance of steel and composite connections under combined axial force and bending including group effects: Analytical procedures and comparison with laboratory tests. Journal of Constructional Steel Research 2019; 160: 320–331

[10] Gil-Martín L.M., Hernandez-Montes E. "A compact and simpler formulation of the component method for steel connections". Journal of Constructional Steel Research 2020; 164. DOI: https://doi.org/10.1016/j.jcsr.2019.105782

[11] Chenaghlou M.R., Nooshin H. Axial force–bending moment interaction in a jointing system part I: (Experimental study), Journal of Constructional Steel Research 2015; 113: 261–276

[12] Chenaghlou M.R., Nooshin H. Axial force–bending moment interaction in a jointing system part II: Analytical study, Journal of Constructional Steel Research 2015; 113: 277–285

[13] Fan F., Ma H., Chen G., Shen S. Experimental study of semi-rigid joint systems subjected to bending with and without axial force. Journal of Constructional Steel Research 2012; 68: 126–137

[14] Yang J.G., Murray T.M., Plaut R.H. Three-dimensional finite element analysis of double angle connections under tension and shear. Journal of Constructional Steel Research 2000; 54: 227–244.

[15] Citipitioglu A.M., Haj-Ali R.M., White D.W. Refined 3D finite element modelling of partially-restrained connections including slip. Journal of Constructional Steel Research 2002; 58: 995–1013.

[16] Augusto H., Simões da Silva L., Rebelo C., Castro J.M. Characterization of web panel components in double-extended bolted end-plate steel joints. Journal of Constructional Steel Research 2016; 116: 271–293

[17] Girão-Coelho A. M., Bijlaard F.S.K. Finite element evaluation of the strength behaviour of high-strength steel column web in transverse compression. Steel and Composite Structures 2010, 10 (5): 385–414

[18] Bayo E, Loureiro A, Lopez M, Shear behaviour of trapezoidal column panels. I: Experiments and finite element modelling. Journal of Constructional Steel Research 2015; 108: 60–69
[19] Lopez M., Loureiro A., Bayo E. Shear behaviour of trapezoidal column panels. II: Parametric study and cruciform element. Journal of Constructional Steel Research 2015; 108: 70–81
[20] Loureiro A., Lopez M, Bayo E. Shear behaviour of stiffened double rectangular column panels: Characterization and cruciform element. Journal of Constructional Steel Research, 2016; 117: 126–138
[21] Bayo E., Gracia J. "Stiffness modelling of 2D welded joints using metamodels based on mode shapes". Journal of Constructional Steel Research 2019; 156: 242-251
[22] CEN. Eurocode 3 - Design of steel structures - Part 1-5: Plated structural elements. (EN 1993-1-5), 2006.
[23] Jönsson J., Stan T.C. "European column buckling curves and finite element modeling including high strength steels". Journal of Constructional Steel Research, 2017; 128: 136–151
[24] Matlab: Statistics and Machine Learning Toolbox. MathWorks Inc., 2017
[25] Kozlowski A., Ziemiański L. "The use of neural networks for identification of parameters of semi-rigid connections". 22nd Australasian Conference on the Mechanics of Structures and Materials, Sydney. 2012. DOI: 10.1201/b15320-147.
[26] De Lima LRO, da S Vellasco PCG, de Andrade SAL, Vellasco MMBR, da Silva JGS. Neural networks assessment of beam-to-column joints. J Braz Soc Mech Sci Eng 2005; 28 (3): 314–24.

TABLES

Table 1
Comparison of moment resistances between the proposed method and EC3

Column	Beam	Steel Grade	$F_{c,Rd}$ (EC3)	$F_{c,Rd}$ (FEM)	Component Failure	M_{Rd} (EC3)	M_{Rd} (FEM)	Error (%)
HEB 200	IPE 330	S275	493.2	487.0	cwc	157.1	158.3	0.8%
HEB 200	IPE 400	S275	507.9	516.2	cwc	196.3	199.5	1.6%
HEB 240	IPE 360	S275	626.6	623.1	cwc	217.6	216.4	0.6%
HEB 240	IPE 450	S275	642.1	663.5	cwc	279.6	288.9	3.2%
HEB 260	IPE 400	S275	681.3	686.4	cwc	263.3	267.2	1.5%
HEB 260	IPE 500	S275	701.7	710.2	cwc	339.6	343.7	1.2%
HEB 280	IPE 360	S275	715.7	712.9	cwc	248.5	247.6	0.4%
HEB 280	IPE 450	S275	732.0	747.5	cwc	318.7	325.5	2.1%
HEB 300	IPE 330	S275	694.2	714.9	bfc	221.1	227.7	2.9%
HEB 300	IPE 400	S275	817.4	815.8	cwc	315.9	315.3	0.2%
HEB 300	IPE 500	S275	830.5	857.4	cwc	402.0	415.0	3.1%
HEB 320	IPE 450	S275	878.3	903.1	cwc	382.4	393.2	2.7%
HEB 320	IPE 550	S275	894.8	926.2	cwc	476.7	493.5	3.4%
HEB 340	IPE 400	S275	929.9	947.0	bfc	359.4	366.0	1.8%
HEB 340	IPE 500	S275	939.2	967.4	cwc	454.6	468.2	2.9%
HEB 340	IPE 600	S275	958.9	1005.9	cwc	557.1	584.4	4.7%
HEB 200	IPE 330	S355	636.7	635.8	cwc	202.8	202.5	0.1%
HEB 260	IPE 400	S355	879.4	876.8	cwc	339.9	338.9	0.3%
HEB 300	IPE 500	S355	1072.2	1081.6	cwc	518.9	523.5	0.9%

Table 2
Comparison with previous tests on webs under compression

Test	Section	h	b_f	t_w	t_f	r	Steel Grade	$f_{y,f}$	$f_{y,w}$	F_{EXP}	F_{FEM}	Error
M2	HEA260	255.3	259.8	7.8	11.8	23.8	S235	300	335	608	578	4.9%
MH4	HEA200	195.9	203.6	7.7	11.2	18.2	S460	512	542	760	808	6.3%
A3	HEA240	230	240	7.5	12.0	21.0	S235	287	286	502	474	5.6%

Table 3
Limit values obtained for HEB200-IPE330 under bending and tension by two paths

	Increasing M				Increasing N_t			
	N_t	M	N_t/N_{Rd}	M/M_{Rd}	N_t	M	N_t/N_{Rd}	M/M_{Rd}
0%	0.00	158.26	0.00	1.00	0.00	158.26	0.00	1.00
10%	139.44	156.50	0.10	0.99	142.34	156.50	0.10	0.99
25%	348.60	146.63	0.25	0.93	349.83	146.63	0.25	0.93
50%	697.19	113.48	0.50	0.72	697.00	113.48	0.50	0.72
75%	1045.79	59.76	0.75	0.38	1045.65	59.76	0.75	0.38
100%	1394.38	0.00	1.00	0.00	1394.38	0.00	1.00	0.00

Table 4
Limit values obtained for HEB200-IPE330 under bending and compression by two paths

	Increasing M				Increasing N_c			
	N_c	M	N_c/N_{Rd}	M/M_{Rd}	N_c	M	N_c/N_{Rd}	M/M_{Rd}
0%	0.00	158.26	0.00	1.00	0.00	158.26	0.00	1.00
10%	120.23	155.66	0.10	0.98	124.74	155.66	0.10	0.98
25%	300.56	145.62	0.25	0.92	302.86	145.62	0.25	0.92
50%	601.13	112.20	0.50	0.71	599.46	112.20	0.50	0.71
75%	901.69	67.46	0.75	0.43	892.00	67.46	0.74	0.43
100%	1202.25	0.00	1.00	0.00	1202.25	0.00	1.00	0.00

Table 5
Limit values obtained for HEB260-IPE400 under bending and tension by two paths

	Increasing M				Increasing N_t			
	N_t	M	N_t/N_{Rd}	M/M_{Rd}	N_t	M	N_t/N_{Rd}	M/M_{Rd}
0%	0.00	267.22	0.00	1.00	0.00	267.22	0.00	1.00
10%	191.10	264.92	0.10	0.99	192.53	264.92	0.10	0.99
25%	477.75	248.59	0.25	0.93	479.95	248.59	0.25	0.93
50%	955.50	192.99	0.50	0.72	955.40	192.99	0.50	0.72
75%	1433.24	103.63	0.75	0.39	1433.19	103.63	0.75	0.39
100%	1910.99	0.00	1.00	0.00	1910.99	0.00	1.00	0.00

Table 6
Limit values obtained for HEB260-IPE400 under bending and compression by two paths

	Increasing M				Increasing N_c			
	N_c	M	N_c/N_{Rd}	M/M_{Rd}	N_c	M	N_c/N_{Rd}	M/M_{Rd}
0%	0.00	267.22	0.00	1.00	0.00	267.22	0.00	1.00
10%	162.51	262.01	0.10	0.98	172.65	262.01	0.11	0.98
25%	396.28	244.35	0.25	0.91	404.00	244.35	0.25	0.91
50%	792.55	187.15	0.50	0.70	793.48	187.15	0.50	0.70
75%	1188.83	114.08	0.75	0.43	1189.52	114.08	0.75	0.43
100%	1585.10	0.00	1.00	0.00	1585.10	0.00	1.00	0.00

Table 7
Limit values obtained for HEB300-IPE500 under bending and tension by two paths

	Increasing M				Increasing N_t			
	N_t	M	N_t/N_{Rd}	M/M_{Rd}	N_t	M	N_t/N_{Rd}	M/M_{Rd}
0%	0.00	414.98	0.00	1.00	0.00	414.98	0.00	1.00
10%	248.55	414.35	0.10	1.00	233.72	414.35	0.09	1.00
25%	621.38	389.36	0.25	0.94	623.38	389.36	0.25	0.94
50%	1242.76	307.04	0.50	0.74	1242.91	307.04	0.50	0.74
75%	1864.14	167.68	0.75	0.40	1863.92	167.68	0.75	0.40
100%	2485.52	0.00	1.00	0.00	2485.52	0.00	1.00	0.00

Table 8
Limit values obtained for HEB300-IPE500 under bending and compression by two paths

	Increasing M				Increasing N_c			
	N_c	M	N_c/N_{Rd}	M/M_{Rd}	N_c	M	N_c/N_{Rd}	M/M_{Rd}
0%	0.00	414.98	0.00	1.00	0.00	414.98	0.00	1.00
10%	200.23	404.04	0.10	0.97	202.71	404.04	0.10	0.97
25%	500.56	371.70	0.25	0.90	506.49	371.70	0.25	0.90
50%	1001.13	283.82	0.50	0.68	994.85	283.82	0.50	0.68
75%	1501.69	172.30	0.75	0.42	1501.58	172.30	0.75	0.42
100%	2002.25	0.00	1.00	0.00	2002.25	0.00	1.00	0.00

FIGURES

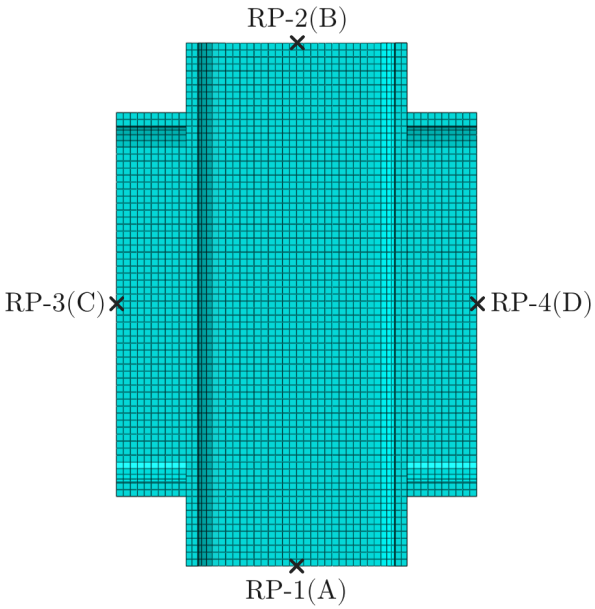

Fig. 1. Finite element model and situation of the reference points.

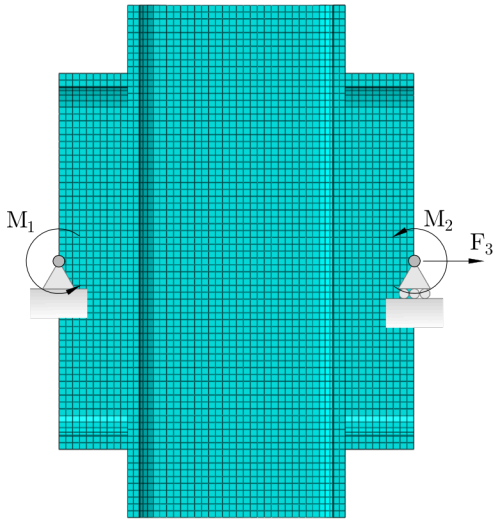

Fig. 2. FEM model boundary conditions and load introduction.

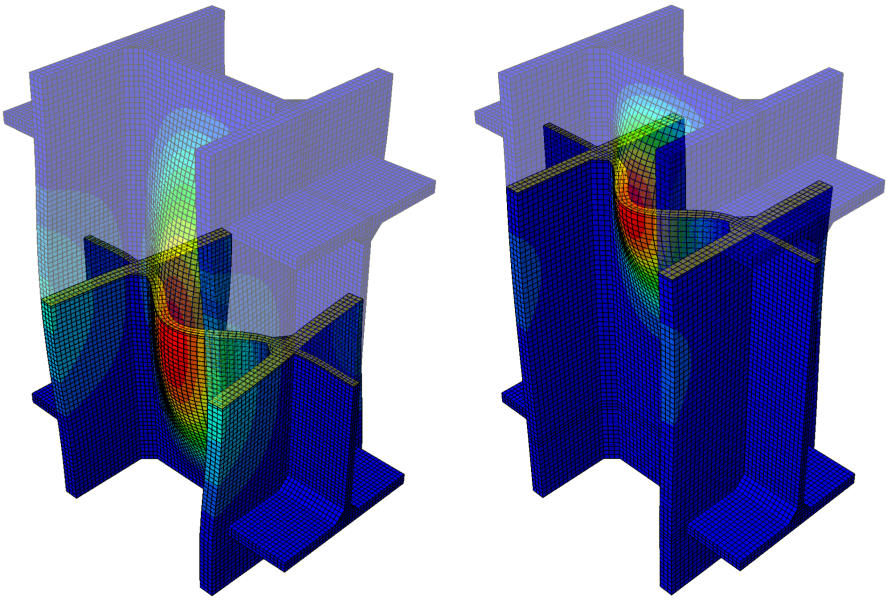

Fig. 3. First Buckling modes for HEB200 - IPE330 model: a) axial compression b) sagging bending moment.

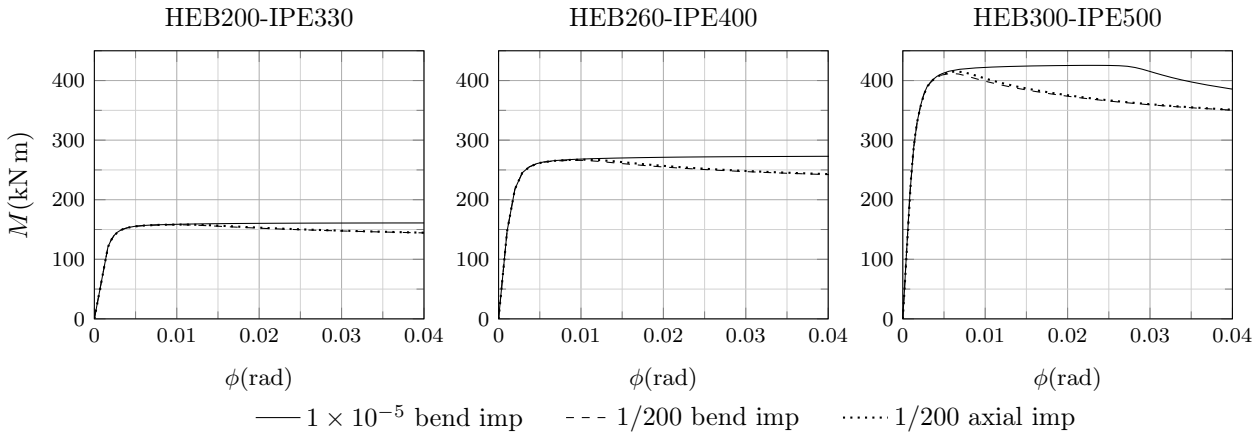

Fig. 4. Moment-rotation curves for different initial imperfections.

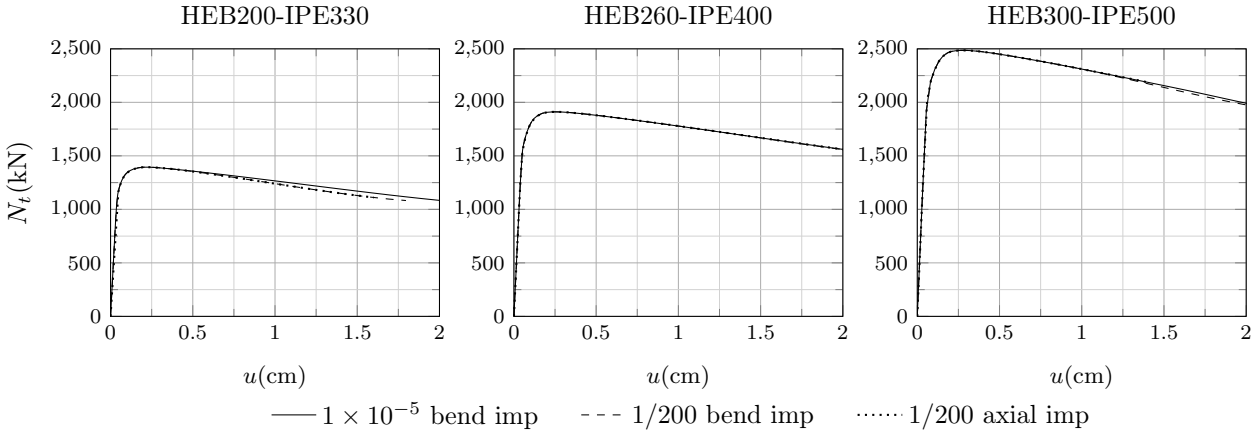

Fig. 5. Tension force-displacement curves for different initial imperfections.

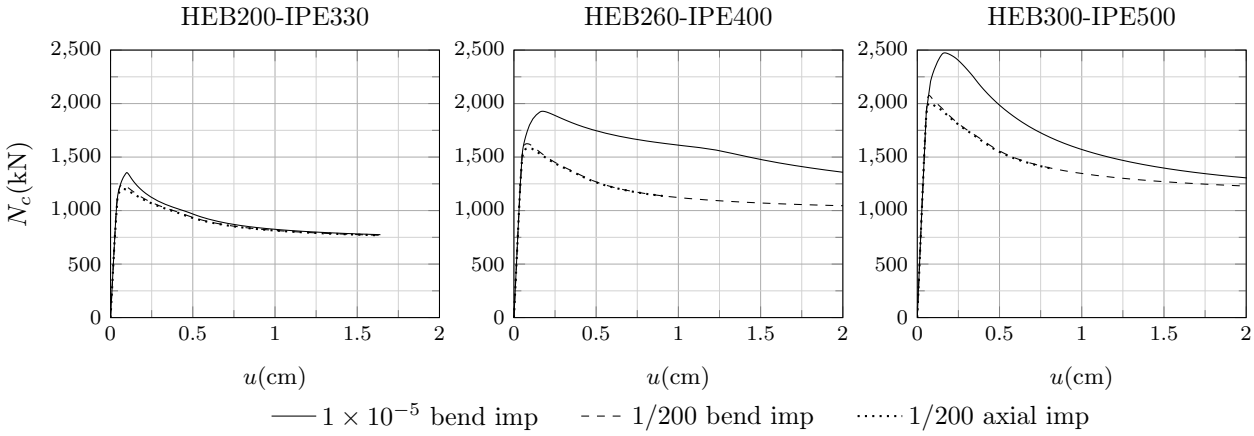

Fig. 6. Compression force-displacement curves for different initial imperfections.

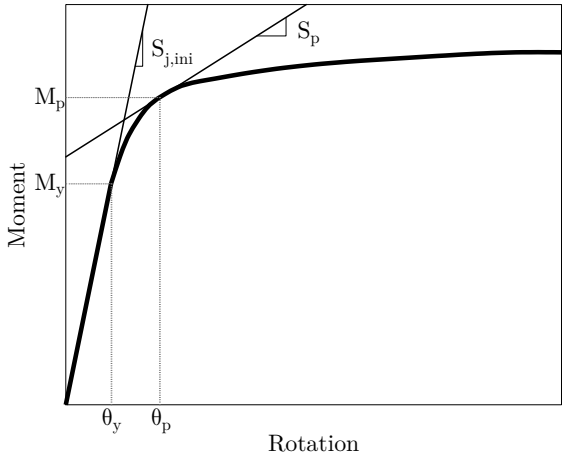

Fig. 7. Characterization of the moment resistance M_{Rd}.

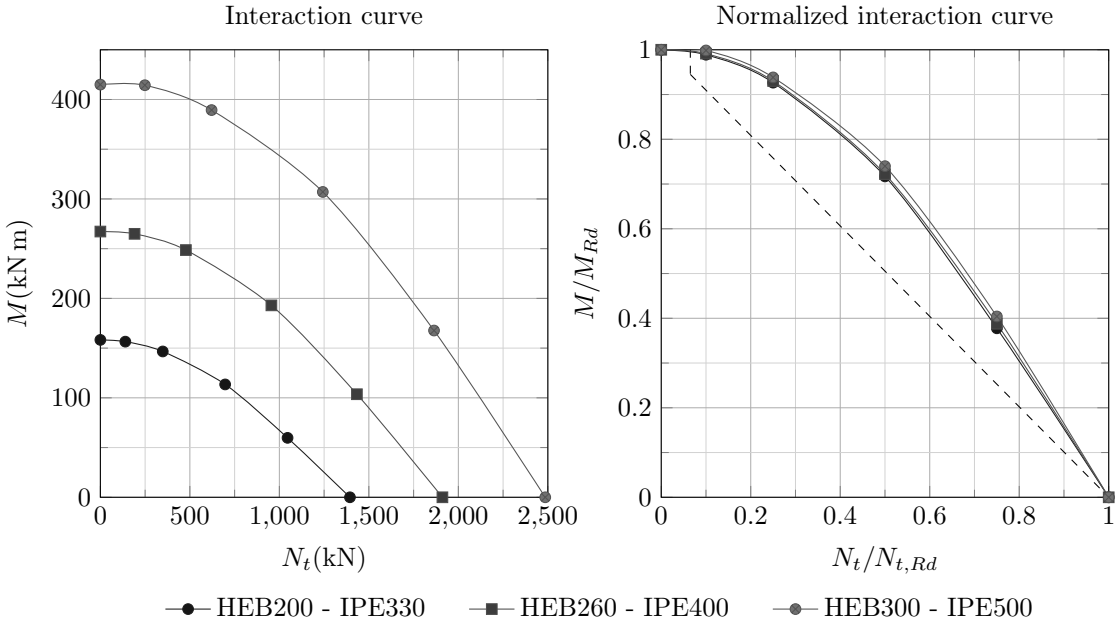

Fig. 8. Interaction curve between bending moment and axial tension force. The diagonal line corresponds to the current Eurocode 3 interaction relation.

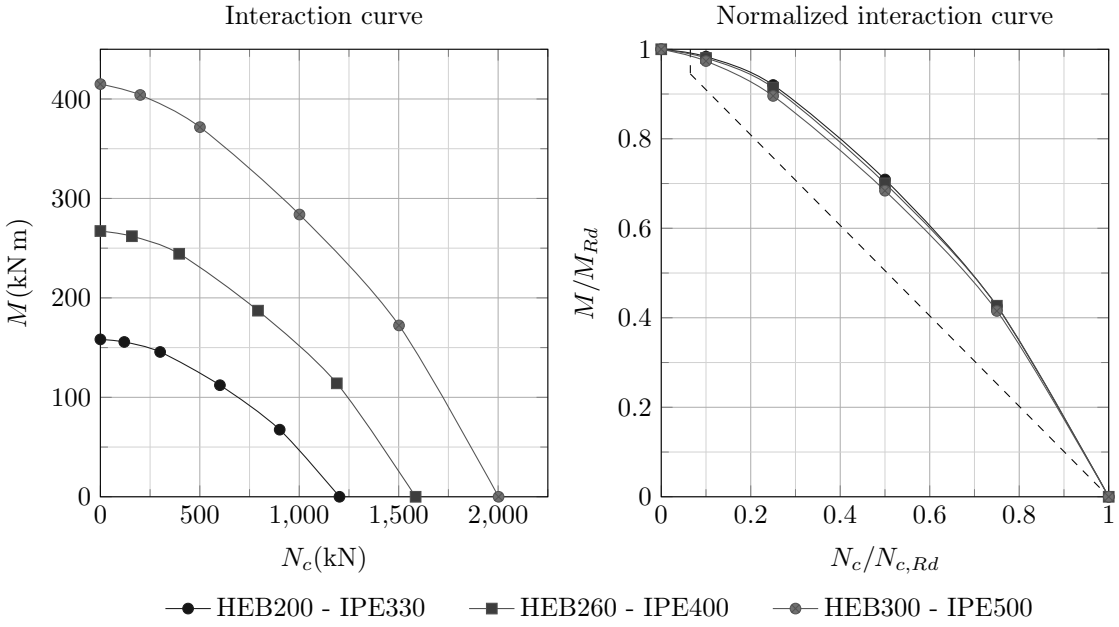

Fig. 9. Interaction curves between bending moment and axial compressive force. The diagonal line corresponds to the current Eurocode 3 interaction relation.

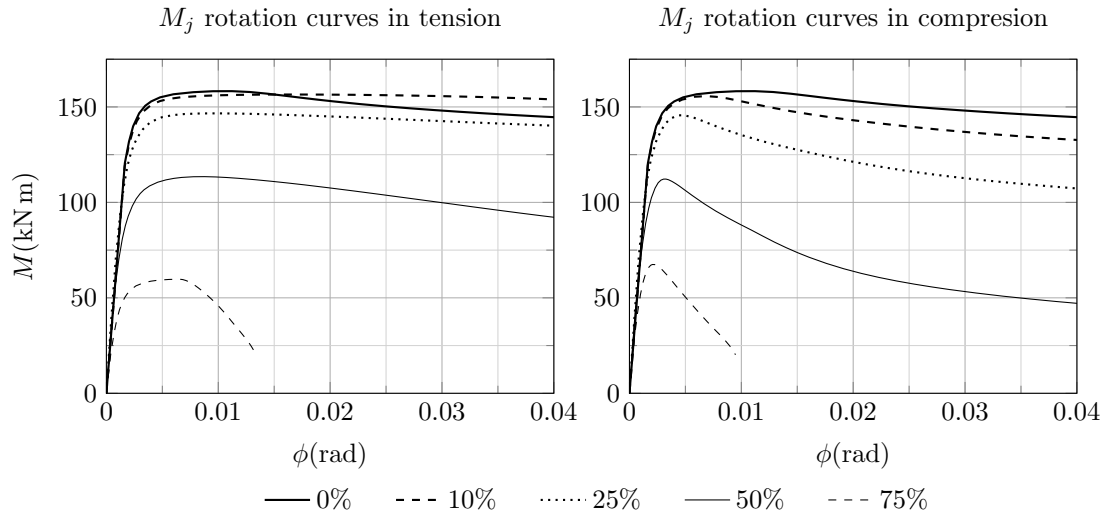

Fig. 10. Moment-rotation curves (HEB200-IPE330) for different axial loads.

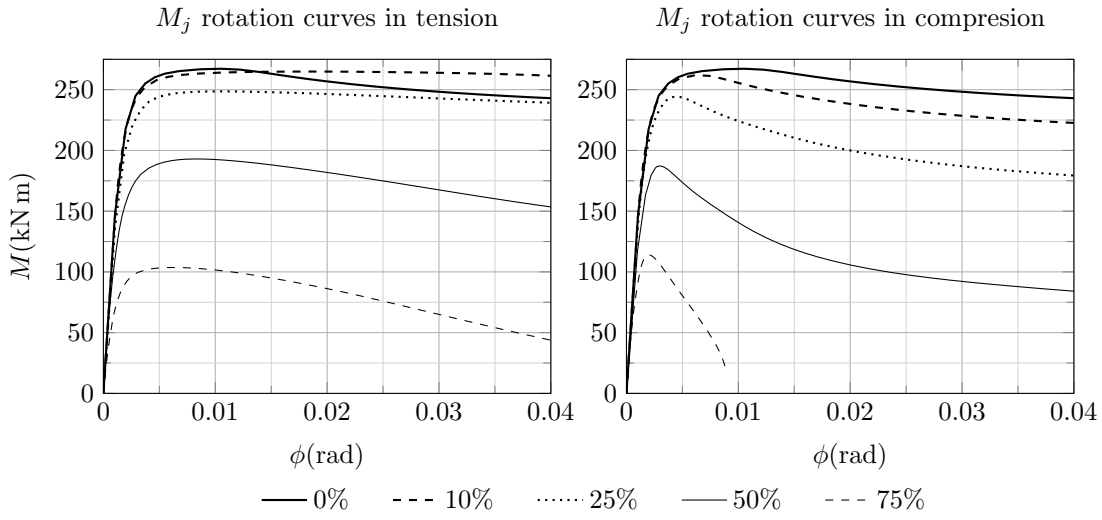

Fig. 11. Moment-rotation curves (HEB260-IPE400) for different axial loads.

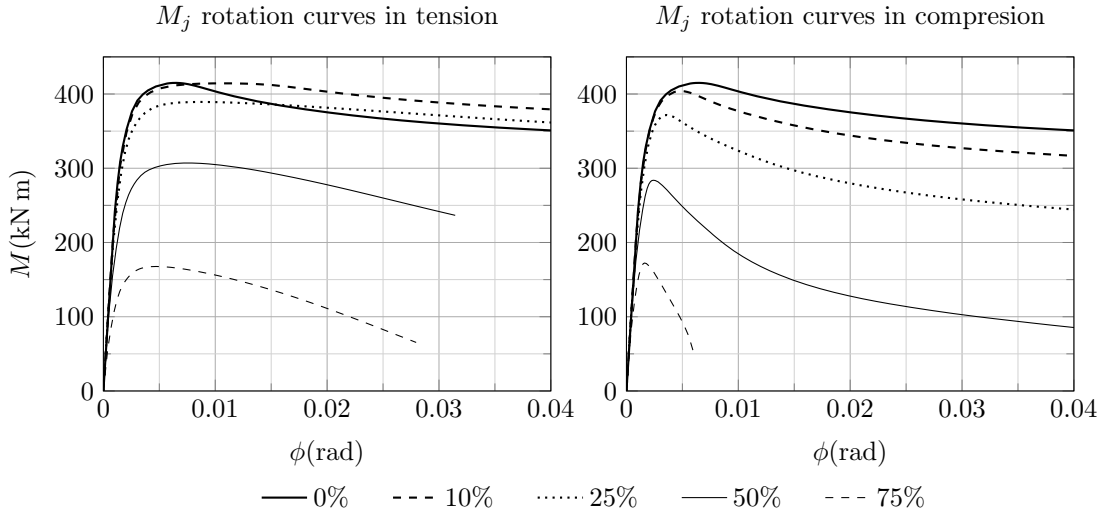

Fig. 12. Moment-rotation curves (HEB300-IPE500) for different axial loads.

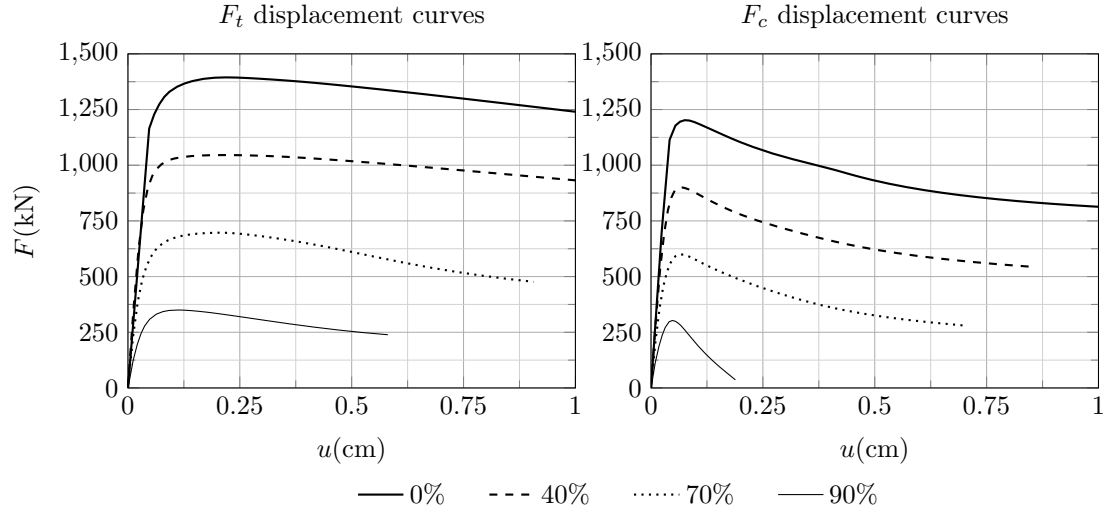

Fig. 13. Force-displacement curves (HEB200-IPE330) for different bending loads.

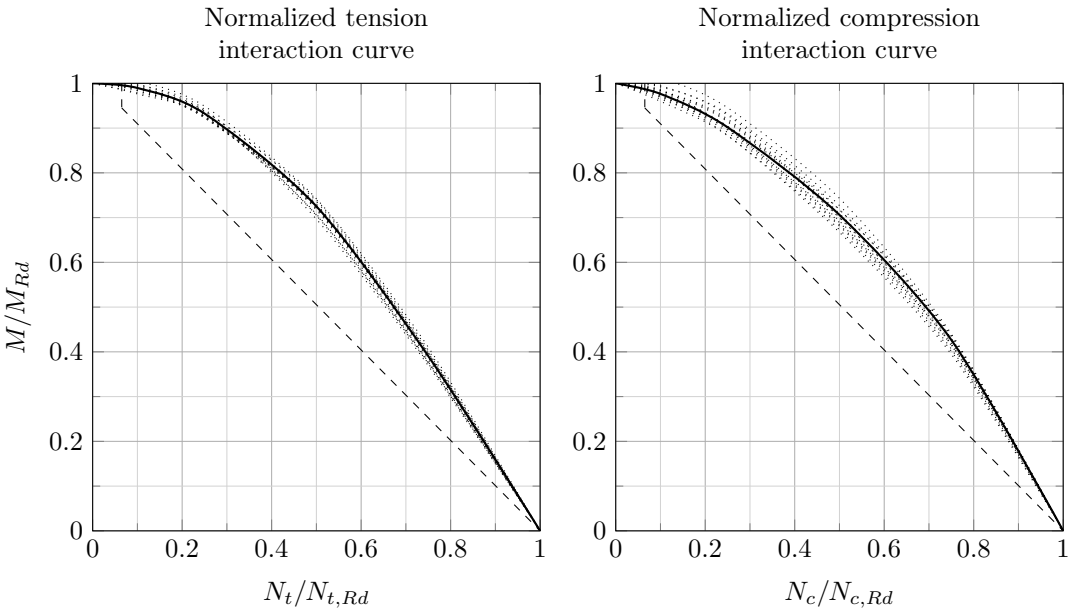

Figure 14. Normalized interaction curves for the sample cases. The diagonal line corresponds to the current Eurocode 3 interaction relation.